# Solvatomorphism-induced 45 K hysteresis width in a spin-crossover mononuclear compound

Abdelhak Djemel, Olaf Stefánczyk, Mathieu Marchivie, Elzbieta Trzop, Eric Collet, Cédric Desplanches, Rachid Delimi, Guillaume Chastanet

# Solvatomorphism-Induced 45 K Hysteresis Width in a Spin Crossover Mononuclear Compound

Abdelhak Djemel[a,b], Olaf Stefanczyk[a], Mathieu Marchivie[a],*, Elzbieta Trzop[c], Eric Collet[c], Cédric Desplanches[a],*, Rachid Delimi[b], Guillaume Chastanet[a],*

**Abstract:** Spin transition compounds are coordination complexes that can present two stable or metastable high-spin and low-spin states at a given temperature (thermal hysteresis). The width of the thermal hysteresis (difference between the maximum and minimum temperature between which the compound exhibits bistability) depends on the interactions between the coordination complexes within the compound, and which may be modulated by the absence or presence of solvent within the structure. The new compound $[Fe(3\text{-}bpp)_2][Au(CN)_2]_2$ (**1**) was synthesized and its properties were compared with those of the solvated compound $[Fe(3\text{-}bpp)_2][Au(CN)_2]_2.2H_2O$ (**1.H$_2$O**) already described. **1** has a two steps thermal hysteresis of 45 K, in contrast to the compound **1.H$_2$O** which exhibits a gradual conversion without hysteresis. This hysteretic transition is accompanied by a reversible reconstructive structural transition and twinning. This stepped behaviour is also observed on the photomagnetic properties despite the low efficiency of photoswitching. Single-crystal photocrystallographic investigations confirm this low conversion which we attributed to the high energy cost to form the high spin structure whose symmetry differs from the one of the low spin phase.

## Introduction

Switching phenomenon of molecular based materials is an open challenge for synthetic chemists.[1] Among potential phenomena, spin state switching upon external perturbation offers memory effect sought for data processing or sensors. Spin-crossover (SCO) complexes of $3d^4$ to $3d^7$ metal ions, displaying high-spin (HS) ↔ low-spin (LS) transition upon temperature, light, pressure, chemical or magnetic field perturbations, are typical examples of such switching abilities. Therefore, they have focused a huge amount of investigations in the last 80 years because of potential involvement in devices.[2] Most of the explored systems are pseudo-octahedral $3d^6$ iron(II) complexes that may be either paramagnetic (HS, S = 2) or diamagnetic (LS, S = 0).

In SCO materials, memory effect is mainly promoted by elastic interactions responsible of cooperative transformation and thermal hysteresis loop.[3] These interactions can be assisted by the formation of extended polymeric architectures or by supramolecular assembly of mononuclear complexes. Such intermolecular interactions are mediated by hydrogen or halogen bonds, Van der Waals interactions, aromatic overlap… which are usually weak compared to chemical bond that lead to polynuclear extended networks. Extended networks built on bridging ligands often exhibit thermal hysteresis loops, up to 88 K wide. [4] However, the widest hysteresis loops are found in mononuclear compounds, up to 140 K wide[5], sometimes accompanied by structural phase transitions. The most cooperative compounds belong to homoleptic complexes based on tris-heterocyclic N,N,N-tridentate ligand which is case of the bpp family (2,6-di-(1*H*-pyrazol-1-yl)pyridine, 1-bpp or 2,6-di-(1*H*-pyrazol-3-yl)pyridine, 3-bpp) which is a highly documented family.[6] In many cases and in particular with the homoleptic bis-tridentate iron(II) complexes, solvatomorphs show very different spin crossover properties.[5,7] This follow from the fact that the solvent molecules inserted in the crystal packing could favour or not the intermolecular interactions. Usually, upon solvent removal, more cooperative transitions are observed. Complexes of the bpp family often show thermal spin crossover close to room temperature or with hysteresis loops. As part of the search for large room temperature centred hysteresis for data processing, this family is intrinsically interesting. Since hysteresis result from cooperative interactions, intermolecular interactions should be favoured. In that context, the 3-bpp ligand possesses an H atom linked to one nitrogen of the pyrazolyl ring free for hydrogen bonding with the anions. While many halogenate or oxide anions have been investigated, few examples report the use of cyanide-based anions.

$[M(CN)_2]^-$ (M = Ag, Au) anions have been widely used to synthesize extended systems presenting spin crossover properties [8]. In this paper we reinvestigate a compound synthesized by Halcrow and coworkers, the $[Fe(3\text{-}bpp)_2][Au(CN)_2]_2.2H_2O$ (**1.H$_2$O**) in which $[Au(CN)_2]^-$ anions acts as a counter-anion.[9] This compound crystallizes in the monoclinic $P2_1/c$ space group. Due to aurophilic interactions between the anions and to anionic disorder, a more rigorous formula was proposed as $[Fe(3\text{-}bpp)_2]_2[Au(CN)_2][Au_3(CN)_6].2H_2O$. The absence of direct hydrogen bonding or strong π-π interactions between the iron centres was consistent with an incomplete and gradual spin crossover from a LS state at 100 K to a mixture of HS and LS molecules at 300 K. We decided to reinvestigate this compound with the idea of using the $[Au(CN)_2]^-$ dicyanide-based anion to

[a] Mathieu Marchivie, Cédric Desplanches, and Guillaume Chastanet, CNRS, Université de Bordeaux, ICMCB, 87 avenue du Dr. A. Schweitzer, Pessac, F-33608, France, guillaume.chastanet@icmcb.cnrs.fr; cédric.desplanches@icmcb.cnrs.fr; mathieu.marchivie@icmcb.cnrs.fr
[b] Abdelhak Djemel, Rachid Delimi, Laboratoire de Traitement des Eaux et Valorisation des Déchets Industriels, Université Badji Mokhar, Annaba, Algérie.
[c] Elzbieta Trzop and Eric Collet, Univ Rennes 1, CNRS, Institut de Physique de Rennes, UMR 6251, F-35042 Rennes, France

promote strong and directional intermolecular interactions to enhance the cooperativity of the materials. To insure short contacts between the 3-bpp ligand and the anions, solvent molecules should be avoided. Several crystallisation conditions were tested to obtain the $[Fe(3\text{-bpp})_2][Au(CN)_2]_2$ desolvated phase. This phase was structurally and magnetically investigated. Huge behaviour differences between the two solvatomorphs **1** and **1.H₂O** were observed and are described in this paper. In **1**, the aurophilic interactions between the anions were evidenced to play a key role in the appearance of a structural phase transition.

## Results and Discussion

**Synthetic strategy.**

The 3-bpp ligand (2,6-di-(1*H*-pyrazol-3-yl)pyridine) has been synthesized according to the previously reported method.[10] Compound **1** has been synthesized by slow diffusion of an aqueous solution of $KAu(CN)_2$ into a methanolic solution of $FeSO_4.6H_2O$ and bpp ligand without further recrystallization. Compound **1**·$H_2O$ synthesized by Halcrow and co-workers was synthesized using water as the only solvent, the compound being then recrystallized from 2,2,2-trifluoroethanol/diethyl ether.[9] Chemical analysis are in favour of the absence of solvent molecules in the structure.

**Magnetic properties**.

Magnetic measurements were recorded on an assembly of monocrystals of compound **1**. Figure 1 reports the evolution of the $\chi_M T$ product ($\chi_M$ being the molar magnetic susceptibility and T the temperature). At room temperature, the $\chi_M T$ product is 0.3 $cm^3$ K $mol^{-1}$, in agreement with a LS state for the iron(II). Upon warming, $\chi_M T$ product slightly increases up to 1.0 $cm^3$ K $mol^{-1}$ at 415 K. At this temperature an abrupt increase of $\chi_M T$ occurs in two steps to reach at 450 K a $\chi_M T$ value of 4.1 $cm^3$ K $mol^{-1}$, suggesting that Fe(II) is fully in high spin state. Upon cooling, $\chi_M T$ remains essentially constant down to 424 K then decreases to reach 3.5 $cm^3$ K $mol^{-1}$ at 418 K. The $\chi_M T$ value remains quasi constant down to 380 K where an abrupt decrease is observed, reaching 0.5 $cm^3$ K $mol^{-1}$ at 340 K, temperature at which most of the Fe(II) are in low spin state.

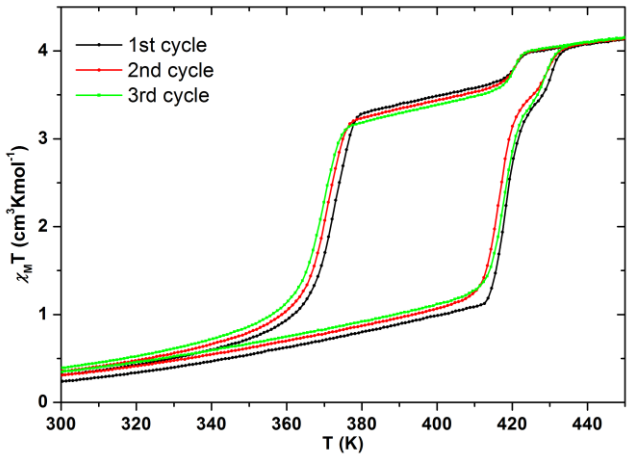


Figure 1. Thermal dependence of the $\chi_M T$ product of **1**.

Three cycles were recorded and the measurements are clearly reproducible. The magnetic properties can thus be described as the superposition of two hysteresis cycles. About 85 % of iron centres have their magnetic behaviour described by the major cycle, having $T_{1/2\downarrow}$ = 370 K and $T_{1/2\uparrow}$ = 415 K. The remaining 15 % of iron centres have their magnetic behaviour described by a smaller hysteresis cycle with $T_{1/2\downarrow}$ = 420 K and $T_{1/2\uparrow}$ = 430 K. The hysteresis width is thus about 45 K for the major hysteresis and about 10 K for the minor one. One may notice the presence of a background slope in the $\chi_M T$ curve below 400 K on the warming branch and above 420 K in the cooling branch of the hysteresis. This slope could follow from i) a bad diamagnetic correction, ii) a strong TIP (Temperature Independent Paramagnetism) contribution, iii) the presence of the hydrated **1**.$H_2O$ phase. The diamagnetic contribution of the sample holder was made using by subtracting its contribution measured without the sample in order to minimize the error. Moreover, after several warmings up to 440 K the slope remains the same. Above this temperature, water should be removed from the structure and the slope, if due to the hydrated phase, should disappear, which is not the case. The presence of this slope is most likely due to a strong TIP contribution.

Compound **1** presents thus a drastic difference when compared with compound **1**.$H_2O$ reported by Halcrow and co-workers.[9] Indeed compound **1**.$H_2O$ presents a very gradual spin crossover with a very smooth and partial conversion between 200 and 300 K. The conversion is incomplete, the high spin fraction at 300 K being only about 55-60 %. The remarkable solvatomorphism observed for compound **1** thus leads to a very strong change in cooperativity for the compound. The presence of two steps in the hysteresis loop does not come from the presence of a small amount of **1**.$H_2O$ since their SCO properties are drastically different. Moreover, the magnetic measurement were performed on an assembly of monocrystals and, as discussed below, no other phases of **1** was observed, as confirmed by powder diffraction (figure S6 of the supplementary information).

Such solvatomorphism has been reported on many compounds to affect the magnetic properties, especially on the $[Fe(bpp)_2]^{2+}$ family [6,7] and sometimes with remarkable changes in other bis-tridentate homoleptic complexes.[5]

**Crystal structure.**

The crystal structure of compound **1** has been solved at 120, 400, 418 and 440 K in the warming up mode and at 428, 410, 390 and 360 K in the cooling mode. It crystallizes in a C2/c monoclinic space group at each temperature but undergoes a reconstructive structural transition above 416 K on warming and below 370K on cooling (Table 2 in experimental section). Above 416K on warming, the compound undergoes a sharp structural transition between two C2/c space groups. The principal modification due to this structural transition corresponds to a strong variation of the β angle of the corresponding primitive cell (Table 2). It can be seen in Figure 2 that translation symmetry changes from the low temperature crystal lattice a,b,c to the a',b',c' high temperature lattice**.** As the monoclinic axis changes direction, this phase transition is reconstructive, without group-subgroup relationship between the two phases and the phase transition is therefore first-

order. Moreover, this phase transition is reversible since upon cooling, the low temperature phase is recovered below 370K. This unusual behaviour is discussed in details below.

In the low temperature phase at 120 K and 400 K, the asymmetric unit is constituted by one $[Fe(bpp)_2]^{2+}$ cation and two $[Au(CN)_2]^-$ anions (figure 3). These two anions form a dimer thanks to an aurophilic interaction that become weaker at 400K ($d_{Au-Au}$ = 3.2164(2) and 3.3989(1) Å respectively at 120 K and 400 K). The angle between the two $[Au(CN)_2]^-$ anions is about 65° at both temperatures. Dimers are strongly linked to four $[Fe(bpp)_2]^{2+}$ cations by H-bond involving the CN group with the N-H of the pyrazole part of the bpp ligands leading to a supramolecular 2D arrangement within the **bc** plane (figure 4).

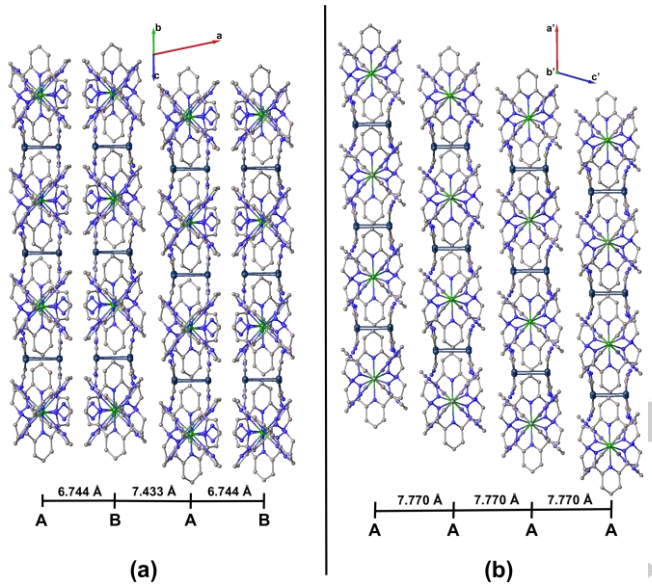


**Figure 2:** View of the crystal packing of **1** showing the successive supramolecular 2D planes (a) in the LS state at 120 K along the [011] crystallographic direction and (b) in the HS state at 418 K along **b**.

A weaker aurophilic interaction within a direction close to the **a** parameter is also present betwen two dimeric anions ($d_{Au-Au}$ = 3.5994(1) and 3.6636(1) Å respectively at 120 K and 400 K) leading to dimers of 2D planes, the crystal structure can be described along the [011] direction as a succession of 2D planes A:B···A:B where A:B represent the dimeric supramolecular 2D planes (figure 2a). Dimers are connected to each other by Van der Waals interactions between the $[Au(CN)_2]^-$ anion and the bpp ligand and by direct π stacking interactions between two $[Fe(bpp)_2]^{2+}$ cations (table S1 in supplementary information).

**Table 1:** Iron environment at 120 K, 400 K, 418 K and 440 K.

| Temperature /K | 120 | 400 | 418 | 440 |
|---|---|---|---|---|
| <dFe1-N> /Å | 1.954(2) | 1.991(5) | 2.105(18) | 2.115(18) |
| <dFe2-N> /Å | | | 2.111(18) | 2.117(19) |
| Σ[a] (Fe1) /° | 99(1) | 107(2) | 143(9) | 143(10) |
| Σ[a] (Fe2) /° | | | 134(8) | 133(8) |
| Vp[b] (Fe1) /Å$^3$ | 9.6(1) | 10.0(1) | 11.5(3) | 11.7(3) |
| Vp[b] (Fe2) /Å$^3$ | | | 11.7(3) | 11.9(3) |

[a]Σ is the sum of the deviation from 90° of the 12 cis-angles of the $FeN_6$ octahedron[11]; [b]Vp is the volume of the octahedron around the metal center.

The iron environment corresponds to a pseudo octahedral geometry, even if the $FeN_6$ octahedron is significantly distorted, the Fe-N bond lengths, octahedron volume and Σ parameter (1.954(2) Å, 9.6(1) Å$^3$ and 99(1) ° respectively, table 1) correspond to the expected values for a LS Fe(II) in this series of $[Fe(bpp)_2]^{2+}$ complexes.

The structural transition corresponds to the disappearing of the weakest aurophilic interaction due to a strong gliding of the plane B within the **b** direction (400 K unit cell) or **a'-b'** (418 K unit cell) with respect to the A plane (figure S1) leading to a new structural arrangement that can be described along the new **b'** direction as a succession of equidistant supramolecular 2D planes A···A without dimerization (Figure 2b). As the gliding can occur in two opposite directions, the crystal presents twinned domains related by a macroscopic 2 fold axis along the **a'+b'**

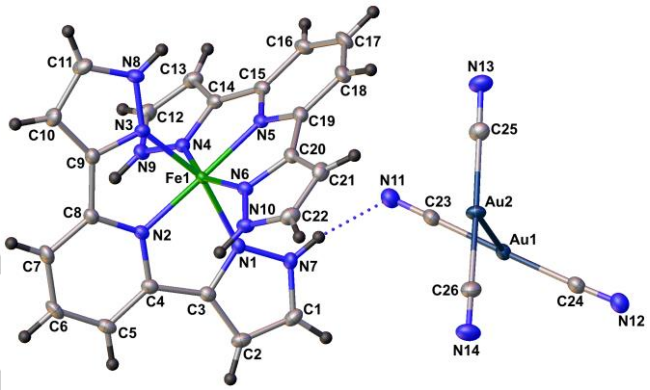


**Figure 3:** Asymmetric unit of **1** at 120K in the LS state showing the labelling scheme. The thermal ellipsoids are represented with 50% probability.

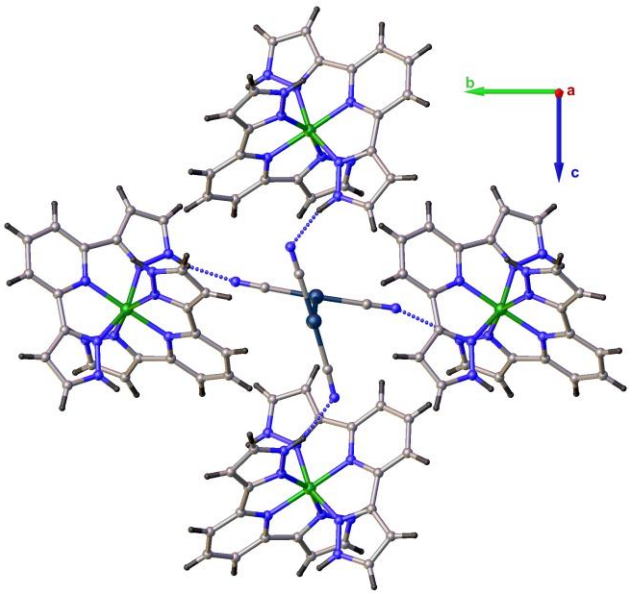


**Figure 4**: view of the crystal structure of **1** at 120K in the LS state along the [100] crystallographic direction showing the H-bonding interactions between the $[Au(CN)_2]^-$ dimer and 4 neighboring $[Fe(bpp)_2]^{2+}$ cations. Color code : Au: dark blue, C: gray, Fe: green, H: black, N: blue.

crystallographic direction (figure S2). The crystal structure should then be solved according to the corresponding twin law with the domain proportion refined to ca. 50%. The supramolecular 2D A planes are constructed in the same way that before the transition,

where each anion form a dimer by aurophilic interaction, which is connected to four $[Fe(bpp)_2]^{2+}$ cations by H-bonding. The aurophilic interaction that tended to weakening just before the structural transition is clearly reinforced by the new structural arrangement as Au-Au distance goes from 3.3989(1) Å before the transition to 3.2814(2) Å at 418 K. Additionally the angle between the two $[Au(CN)_2]^-$ anions increase to ca. 90°.

It is worth to note that this structural transition leads to two different sites for the iron atom both of them situated on a 2-fold axis. The asymmetric unit is then constituted of two half $[Fe(bpp)_2]^{2+}$ cations and two $[Au(CN)_2]^-$ anions (figure S3). At 418 K both iron environments correspond to distorted octahedral geometry, the Fe-N bond lengths, octahedron volume and Σ parameter are respectively 2.105(18) Å, 11.5(3) Å$^3$ and 143(9)° for Fe1 and 2.111(18) Å, 11.7(3) Å$^3$ and 134(8)° for Fe2. These values indicate that both iron atom are close to the HS state, the structural transition is then concomitant with a sharp SCO for this compound. Nevertheless, even if the SCO occur on both iron sites, they behave independently because of the symmetry breaking and the two steps may be related to two thermal conversions. At 440 K, the iron environments slightly move, but the bond lengths precision is not sufficient to accurately know if both sites are affected in the same way (table 1).

The crystal structure solved during the cooling mode revealed a slight difference of the two iron environments but the metals remain close to the HS state till 390 K with a similar independent behaviour. These small differences in the modification of coordination sphere of the metal centres, have to be very carefully taken into account as, due to the damaging of the crystal during the transition, and the domain formation, the precision of the different crystal structures is poor and observed variations lie into the standard deviations. However the symmetry change revealed by X-ray diffraction clearly show that two different sites exists on the step. Below 370 K the crystal undergoes a structural transition back to the low temperature LS crystal structure at 360 K with the potential disappearing of the twined domains.

The SCO is thus accompanied by a reversible reconstructive structural transition leading to 2 independent iron sites in the HS state and on the step and only 1 site in the LS one. Also, this structural transition induces potentially reversible domains formation in the crystal which is due to a strong gliding of 2D supramolecular planes occurring in 2 opposite directions with the same probability.

Compared to the previously described **1.H₂O**, the crystal structure of **1** is clearly more compact as 2D supramolecular planes that are also observed in **1.H₂O** are separated by an extra $[Au(CN)_2]^-$ anion interacting with the $H_2O$ molecule that move the 2D planes away from each other. Consequently, the 2D supramolecular planes in **1** are much closer and interact much strongly than in the parent hydrated compound ($d_{A:B}$ = 6.7438(2) and 9.835(3) for **1** and **1.H₂O** respectively, figure S4). The close contacts of the A:B plane in **1** may then be responsible of the structural transition at the SCO due to the increase of the molecular volume of the $[Fe(bpp)_2]^{2+}$ cation explaining the strong cooperativity and the large hysteresis loop of the anhydrous compound. As the structural transition is leading to 2 independent Fe(II) sites above 416 K, both iron sites may behave differently after the transition, which is potentially clarifying the multistep transition as related to the formation of spin-state concentration waves [12]. Even though X-ray data hardly distinguish the spin state concentration on each site (because of domain formation), the small 10K hysteresis loop corresponding to the 10 – 15 % last of the spin crossover clearly identify two steps. Additionally, it is worth noting that a small part of the diffraction pattern can be still indexed in the original a,b,c crystal lattice even after the transition. The HS crystal structure is thus constituted of two coexisting phases with different lattices: the main phase corresponding to the a',b',c' crystal lattice with the domains formation due to the reconstructive phase transition and the minor one where the crystal remains in the initial a,b,c crystal lattice. This later minor phase could also explain the smaller secondary hysteresis loop at higher temperature as it may correspond to a SCO with a higher $T_{1/2}$ and a smaller cooperativity (no structural transition).

This conclusion is supported by the evolution of the unit cell volume of the main phase that does not reveal any step in the warming and cooling mode (figure S5). Moreover, this small 10 K hysteresis at higher temperature cannot come from the presence of polymorphism in the raw product as only one polymorph is detected by powder X-ray diffraction before the structural transition (Figure S6). The large structural reorganization due to sliding of layers in the lattice and the reconstructive phase transition plays a very important role for the first-order nature of the phase transition.

**Photomagnetic properties.**

Compound **1** was shown to exhibit photomagnetic properties. The properties were recorded following the standard T(LIESST) measurements method[13] and are presented on figure 5. At 10 K, the compound is in low spin state (0.01 cm$^3$ K mol$^{-1}$). When irradiated in situ into the SQUID cavity, $\chi_M T$ increases up to about 1.1 cm$^3$ K mol$^{-1}$, thus about 25 % of iron centres are photoconverted in their high spin state. After a steady state has been reached, irradiation was switched off and the temperature increased

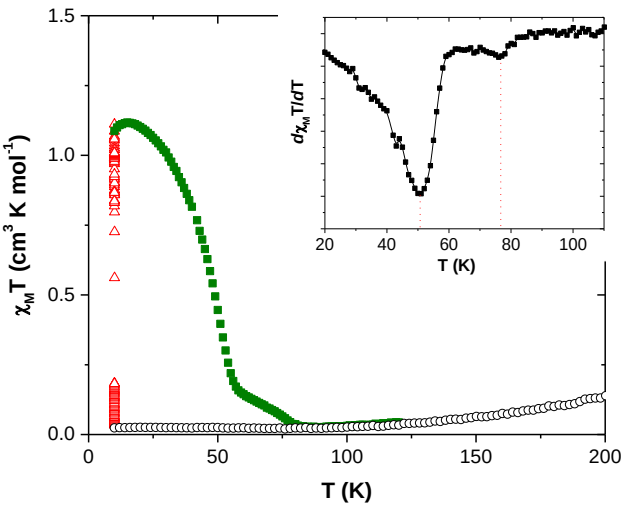


**Figure 5**. thermal dependence of the $\chi_M T$ product of compound **1** before irradiation (o), during irradiation at 650 nm and 5 mW/cm² (Δ) and after irradiation in the dark (■). The inset presents the $d\chi_M T/dT$ derivative.

at 0.3 K $min^{-1}$ while the magnetisation was recorded. A decrease in $\chi_M T$ is observed when the temperature is increased. This decrease occurs in two steps: a first decrease between 10 K and about 50 K, then a second decrease between 50 and 80 K. The first decrease concerns about 80 % of the photoinduced fraction. T(LIESST) is defined as the temperature at which the curve presents an inflection point (minimum of the derivative). In the present case two T(LIESST) values can be defined : one clearly defined at 50 K related to the low temperature relaxation, and the second poorly defined at 75 K, related to the relaxation at high temperature.

Previous studies have demonstrated an empirical relation between $T_{1/2}$ and T(LIESST)[13]: $T(LIESST) = T_0 - 0.3\ T_{1/2}$ with $T_0$ = 150 K for tridentate ligands such as the bpp ligand.[6b,13c,d,e,f, 14] Taking for $T_{1/2}$ the mean value of $T_{1/2\downarrow}$ and $T_{1/2\uparrow}$, $T_{1/2}$ can be evaluated at 392 and 425 K respectively for the two hysteresis cycles. Following the relation between T(LIESST) and $T_{1/2}$, the two T(LIESST) should be about 32 K for the main part of the compound and 22 K for the small part of the compound. The T(LIESST) observed are thus notably higher than the expected values. More surprisingly, the small hysteresis should correspond to the lowest T(LIESST) whereas it seems from the experiment that it is the contrary. A possible explanation for the high temperature component of the LIESST curve is the presence in the sample of a small amount of hydrated compound **1.$H_2O$**. Indeed, **1.$H_2O$** present a very smooth spin crossover, this crossover can be observed at a temperature as low as 200 K, to be compared with the temperatures of 392 and 425 K for $T_{1/2\downarrow}$ and $T_{1/2\uparrow}$ for compound **1**. Following the relationship between T(LIESST) and $T_{1/2}$ already described in this paragraph, T(LIESST) should be higher for **1.$H_2O$** than for **1**. Even if we cannot completely exclude this possibility, the absence of **1.$H_2O$** in the powder diffraction pattern (figure S6) is not in favor of such hypothesis. Photocrystallographic investigations allow to shed some light on this observation.

**Photocrystallographic investigations.**

We attempted to get the crystal structure in the photo-induced HS state by using single-crystal x-ray diffraction at 10 K under laser irradiation. According to reconstructed precession images, the structural transition observed for the thermal SCO, with a change of lattice periodicity, does not seem to take place after irradiation at low temperature as the whole diffraction pattern could be indexed in the initial **a, b, c** LS crystal lattice (Fig S7 and S8). Nevertheless some additional diffuse peaks of very weak intensity could be observed that may correspond to a reconstructive structural transition. However, the photo-induced crystal structure has been solved using the LS unit cell that remains the major phase even after 3.5 hours of irradiation. The crystal structure of the photo-induced state can be described similarly to the LS one at 120 K but with a disordered part around the metal position compatible with the presence of two unresolved $Fe^{2+}$ sites due to the spin transition. The mean Fe-N distance is slightly higher than that expected for a LS state (<dFe-N> = 2.036Å), corresponding to a partial LS to HS conversion of ca. 50% in agreement with the LS and HS ratio within the disordered parts of the photo-induced crystal structure. This partial conversion is in agreement with the photo-magnetic properties and may be due to the large elastic energy cost associated with reconstructive phase transition. This is very likely responsible for the partial structural conversion towards the full HS lattice, as weak energy deposited by light excitation in the lattice may not be enough to overcome the large (elastic) cost due to the sliding of the layers for reaching the HS structure. However, our photocrystallographic studies evidence the presence of a photoinduced structural reconstructive phase transition. Even if this conversion is partial, it may be similar to the one observed at thermal equilibrium. The partial HS conversion may thus result from small HS domains formed by this reconstructive structural transition, associated with the Bragg peaks observed, and/or to a partial conversion in the LS lattice, which seems to be the major phase (conversely to what has been suspected for the thermal SCO). In this way, the two-step relaxation, if not due to the presence of some hydrated phase **1.$H_2O$**, can be seen as similar to the two-steps thermal conversion from the, partially reached, photoinduced HS made of two phases, one coming from a reconstructive transition and a second, partially converted, that remains in the initial crystal lattice corresponding to the major phase. Such a behaviour may explain the two steps relaxation curve observed after irradiation on the magnetic properties on warming as the two different structural arrangements may not correspond to the same T(LIESST). The major phase is associated to the lower T(LIESST) in good agreement with the higher $T_{1/2}$ suspected for the same phase the thermal SCO.

## Conclusions

**1** and **1.$H_2O$** are compounds presenting strongly different spin crossover behaviours. Whereas **1.$H_2O$** presents a very gradual spin-crossover associated with no thermal hysteresis, **1** presents first order spin transition. The differences between **1** and **1.$H_2O$** has been rationalized in terms of compacity of the structures thanks to single crystal X-ray diffraction. This transition can be described as the sum of two hysteresis cycles: a major one having a 45 K width and a minor one having a 10 K width. These compounds are thus nice examples of the influence of solvent of crystallization on physical properties. LIESST effect has also been observed for **1**, showing a thermal decay of the photo-induced high spin into two steps.

## Experimental Section

**Methods.** The starting materials were purchased from Sigma Aldrich and used without further purification. Solvents were used and purified by standard procedures.

**Syntheses.**

$[Fe(3\text{-}bpp)_2][Au(CN)_2]_2$ has been synthesized by slow diffusion in a straight tube. 3 mL of an aqueous solution containing 28.8 mg of $KAu(CN)_2$ has been recovered by 3 mL of a mixture $H_2O$/MeOH. The later was recovered by 3 mL oh methanol solution containing 21.1 mg of 3-bpp ligand and 10 mg of $FeSO_4.6H_2O$. After two weeks, dark red crystals appeared. The yield is about 62 % (47mg). Chemical analysis calculated for $C_{26}H_{18}Au_2FeN_{14}$ (%) C: 31.98, H: 1.86; N: 20.09, obtained (%) C: 31.60, H: 2.03; N:19.72.

**Physical characterizations.**

***Magnetic and Photomagnetic Studies.***
Magnetic measurements were performed on a Microsense EZ7 Vibrating Sample Magnetometer with the 100-1000K EV1-LNA temperature control

option. Samples were weighed in aluminum capsules that were wrapped closed, and glued to a ∅3mm quartz rod with double-face scotch tape. *dc* measurements were performed under 10 kOe magnetic field at a temperature sweeping rate of 10 K/mn. Nitrogen gas flow was used for temperature control. Compared to measurements performed in a MPMS magnetometer in which the sample is under vacuum, the VSM apparatus operates under a constant flow of exchange gas that insure a fast and efficient thermalisation of the sample. Diamagnetic corrections for the sample holder and the material (using Pascal constants) were applied.

Photomagnetic measurements were performed with a set of photo-diodes coupled through an optical fibre to the cavity of a MPMS-55 Quantum Design SQUID magnetometer operating at 2 T. The intensity of irradiation was set to prevent heating of the sample. The crystalline sample was prepared in a thin layer (0.66 mg) to promote full penetration of the irradiated light. Our previously published standardized method for obtaining LIESST data was followed.[13] The sample was first slow cooled to 10 K, ensuring that potential trapping of HS species at low temperatures did not occur. Irradiation was carried out at a set wavelength and the power at the sample surface was adjusted to 5 mW $cm^{-2}$. Once photo-saturation was reached, irradiation was ceased and the temperature increased at a rate of 0.4 $K.min^{-1}$ to ~100 K and the magnetization measured every 1 K to determine the T(LIESST) value given by the extreme of the $\delta \chi_M T / \delta T$ versus T curve for the relaxation. The T(LIESST) value describes the limiting temperature above which the light-induced magnetic high-spin information is erased in a SQUID cavity. In the absence of irradiation, the magnetism was also measured over the temperature range 10 – 290 K to follow the thermal spin transition and to obtain a low temperature baseline.

***Crystallographic investigations.***

Single crystal X-ray studies were performed at 120, 400, 418, 440 K in the warming mode and 428, 410, 390 and 360K in the cooling mode on Xcalibur 2 κ-CCD diffractometer using Mo Kα radiation (λ = 0.71073 Å). The corresponding structures were solved by direct methods with the SHELXS program and refined on $F^2$ by weighted full matrix least- squares methods using the SHELXL program.[15] Both software were used within the OLEX2 package [16], which was also used to construct the figures. All non-hydrogen atoms were refined anisotropically, hydrogen atoms were located in difference Fourier maps and treated using a riding model. The crystal structures above 416 K in the warming mode and above 360K in the cooling mode were solved using a HKL5 format file obtained from TWINABS program [17] to include the contribution of 2 twin domains related by a 180° rotation along the [110] crystallographic direction. Crystallographic data and refinement details are provided in Table 2.

Photocrystallographic single crystal X-ray studies were performed at 10K before and after irradiation with 660nm cw-laser at ~3.5mW laser power on an Oxford Diffraction Xcalibur3 diffractometer, using monochromated

**Table 2:** Crystal data and structure refinement for **1** at different temperatures.

| **Warming up mode** | | | | |
|---|---|---|---|---|
| Temperature/K | 120 | 400 | 418 | 440 |
| Empirical formula | $C_{26}H_{18}Au_2FeN_{14}$ | | | |
| Formula weight | 976.33 | | | |
| Crystal system | monoclinic | | | |
| Space group | C2/c | | | |
| a/Å<br>[*P cell*˚] | 29.5107(9) | 30.4472(10)<br>[*14.2114*] | a'=20.215(4)<br>[*14.295*] | a'=20.222(4) |
| b/Å<br>[*P cell*˚] | 14.2875(4) | 14.2114(5)<br>[*14.3903*] | b'=20.216(4)<br>[*14.295*] | b'=20.223(4) |
| c/Å<br>[*P cell*˚] | 14.2705(5) | 14.3903(5)<br>[*16.8003*] | c'=16.200(3)<br>[*16.200*] | c'=16.251(3) |
| α/°<br>[*P cell*˚] | 90 | 90<br>[*104.386*] | 90<br>[*101.52*] | 90 |
| β/°<br>[*P cell*˚] | 106.093(1) | 105.913(1)<br>[*115.021*] | β '=106.404(6)<br>[*101.52*] | β '=106.315(6) |
| γ/°<br>[*P cell*˚] | 90 | 90<br>[*90*] | 90<br>[*90*] | 90 |
| Volume/Å$^3$ | 5781.1(3) | 5988.0(4) | 6351(2) | 6378(2) |
| Goodness-of-fit on $F^2$ | 1.080 | 0.912 | 1.044 | 1.021 |
| Final R indexes [I>=2σ (I)] | $R_1$ = 0.0141,<br>$wR_2$ = 0.0340 | $R_1$ = 0.0377,<br>$wR_2$ = 0.0770 | $R_1$ = 0.0863,<br>$wR_2$ = 0.2178 | $R_1$ = 0.0922,<br>$wR_2$ = 0.2359 |
| Final R indexes [all data] | $R_1$ = 0.0166,<br>$wR_2$ = 0.0354 | $R_1$ = 0.0856,<br>$wR_2$ = 0.0891 | $R_1$ = 0.1501,<br>$wR_2$ = 0.2680 | $R_1$ = 0.1569,<br>$wR_2$ = 0.2923 |
| **Cooling down mode** | | | | |
| Temperature/K | 428 | 410 | 390 | 360 |
| Crystal system<br>Space group | monoclinic<br>C2/c | | | |
| a/Å | a'=20.226(4) | a'=20.218(3) | a'=20.217(3) | 30.262(6) |
| b/Å | b'=20.230(4) | b'=20.219(3) | b'=20.215(3) | 14.219(3) |
| c/Å | c'=16.226(3) | c'=16.176(3) | c'=16.131(3) | 14.346(3) |
| β/° | β '=106.355(7) | β '=106.415(6) | β '=106.473(6) | 105.885(7) |
| Volume/Å$^3$ | 6371(2) | 6343.3(18) | 6321.7(18) | 5937(2) |
| Goodness-of-fit[a] on $F^2$ | 1.044 | 1.041 | 1.088 | 1.071 |
| Final R indexes[b] [I>=2σ (I)] | $R_1$ = 0.0919,<br>$wR_2$ = 0.2389 | $R_1$ = 0.0894,<br>$wR_2$ = 0.2346 | $R_1$ = 0.0884,<br>$wR_2$ = 0.2348 | $R_1$ = 0.1040,<br>$wR_2$ = 0.2611 |
| Final R indexes [all data] | $R_1$ = 0.1560,<br>$wR_2$ = 0.2934 | $R_1$ = 0.1475,<br>$wR_2$ = 0.2836 | $R_1$ = 0.1416,<br>$wR_2$ = 0.2805 | $R_1$ = 0.1719,<br>$wR_2$ = 0.2976 |
| Photo-crystallography | | | | |
| Temperature/K | 10 - dark | | 10 – after irradiation | |
| Crystal system<br>Space group | monoclinic<br>C2/c | | | |
| a/Å | 29.2828(7) | | 29.3717(8) | |
| b/Å | 14.2963(3) | | 14.1609(3) | |
| c/Å | 14.2441(3) | | 14.2462(4) | |
| β/° | 106.076(2) | | 105.743(3) | |
| Volume/Å$^3$ | 5729.9(2) | | 5703.1(3) | |
| Goodness-of-fit on $F^2$ | 1.038 | | 1.032 | |
| Final R indexes [I>=2σ (I)] | $R_1$ = 0.0250, $wR_2$ = 0.0506 | | $R_1$ = 0.0267, $wR_2$ = 0.0451 | |
| Final R indexes [all data] | $R_1$ = 0.0342, $wR_2$ = 0.0538 | | $R_1$ = 0.0397, $wR_2$ = 0.0490 | |

[c]GooF = $\{\Sigma[w(F_o^2-F_c^2)^2]/(N_{obs}-N_{var})\}^{1/2}$; [b]$R_1 = \Sigma|F_o-F_c|/F_o$. ; $wR_2 = \{\Sigma[w(F_o^2-F_c^2)^2]/\Sigma[w(F_o^2)^2]\}^{1/2}$. ˚Corresponding Primitive cell.

Mo-Kα radiation (λ = 0.71073 Å). The diffractometer was fitted with the Helijet Oxford Diffraction Cryostat working with helium. The corresponding structures were solved by dual-space direct methods with the SHELXT program[18] and refined on $F^2$ by weighted full matrix least- squares methods using the SHELXL program.[15] Both software were used within the OLEX2 package [16], which was also used to construct the figures. All non-hydrogen atoms were refined anisotropically, hydrogen atoms were located in difference Fourier maps and treated using a riding model. Two crystal structures were solved using the cell of the low spin state phase. For the structure of the photo induced HS state the disorder model have been applied for selected C and N atoms at Fe-atom site with 0.5:0.5 ratio of LS/HS state. Crystallographic data and refinement details are provided in Table 2.

CCDC 1828722-1828729 and 1844547-1844548 contain the supplementary crystallographic data. These data can be obtained free of charge from The Cambridge Crystallographic Data Centre via www.ccdc.cam.ac.uk/data_requ- est/cif.

Powder X-ray diffraction (PXRD) patterns were collected on a PANalitycal X'pert MPD-PRO Bragg-Brentano θ-θ transmission geometry diffractometer equipped with a goebel mirror over an angular range of 2θ = 5-40°. The Cu-Kα radiation was generated at 45 KV and 40 mA (lambda = 0.15418 nm). The powder sample was prepared inside a glass capillary.

## Acknowledgements

We thank the CNRS, the University of Bordeaux, the "Agence Nationale de la Recherche" (ANR project BISTA-MAT: ANR-12-BS07-0030-01 ANR project FEMTOMAT: ANR-13-BS04-0002) and “Région Nouvelle Aquitaine” for the funding of this work.

**Keywords:** Coordination Chemistry / Spin-Crossover / Solvatomorphism / Hysteresis / aurophilic interactions / phase transition

[1] a) Spin Crossover in Transition Metal Compounds I−III. In Topics in Current Chemistry; P. Gütlich. H-A. Goodwin, *Eds.; Springer-Verlag: Berlin, Germany*, 2004; Vols. 233−235; b) Spin-crossover materials – properties and applications, ed. M. A. Halcrow, John Wiley & Sons, Chichester, 2013.

[2] a) M. D. Manrique-Juárez, S. Rat, L. Salmon, G. Molnár, C. M. Quintero, L. Nicu, H. J. Shepherd, A. Bousseksou, *Coord. Chem. Rev*., **2016**, *308*, 395; b) K. S. Kumar, M. Ruben, *Coord. Chem. Rev*., **2017**, *346*, 176; c) A. Bousseksou, G. Molnar, L. Salmon, W. Nicolazzi*, Chem. Soc. Rev,* **2011**, *40*, 3313; d) O. Kahn, C.J. Martinez, *Science* **1998**, *279*, 44

[3] a) S. Brooker, *Chem. Soc. Rev*., **2015**, 44, 2880;; b) R. Bertoni, M. Lorenc, H. Cailleau, A. Tissot, J. Laisney, M.-L. Boillot, L. Stoleriu, A. Stancu, C. Enachescu, E. Collet, *Nature Materials,* **2016**, *15*, 606; c) H. Spiering, In Topics in Current Chemistry; P. Gütlich. H-A. Goodwin, *Eds.; Springer-Verlag: Berlin, Germany*, **2004**, *235*, 171.

[4] C. Lochenie, W. Bauer, A. P. Raillet, S. Schlamp, Y. Garcia, B. Weber, *Inorg. Chem*., **2014**, *53*, 11563.

[5] a) T. Buchen, P. Gütlich, K. Sugiyarto, H. Goodwin, *Chem. Eur. J.*, **1996**, *2*, 113; b) M. B. Bushuev, D.P. Pishchur, V. A. Logvinenko, Y. V. Gatilov, I. V. Korolkov, I. K. Shundrina, E. B. Nikolaenkovac, V. P. Krivopalovc, *Dalton Trans*., **2016**, *45*, 107

[6] a) G. Craig, O. Roubeau, G. Aromi, *Coord. Chem. Rev*., **2014**, *269*, 13; b) M.A. Halcrow, *Coord. Chem. Rev*. **2009**, *253*, 2493; c) L.J. Kershaw, R. Mohammed, G. Sherborne, T.D. Roberts, S. Alvarez, M.A. Halcrow, *Coord. Chem. Rev*. **2015**, *289-290*, 2.

[7] a) B. Li, R. Wei, J. Tao, R. Huang, L. Zheng, Z. Zheng, *J. Am. Chem. Soc.*, **2010**, *132*, 1558; b) R. Wei, J. Tao, R. Huang, L. Zheng, *Inorg. Chem.*, **2011**, *50*, 8553; c) R.-J. Wei, B. Li, J. Tao, R.-B. Huang, L.-S. Zheng, Z. Zheng, *Inorg. Chem.*, **2011**, *50*, 1170; d) C. Bartual-Murgui, A. Akou, H. J. Shepherd, G. Molnár, J. A. Real, L. Salmon, A. Bousseksou, *Chem. – Eur. J.*, **2013**, *19*, 15036; e) J. S. Costa, S. Rodríguez-Jiménez, G. A. Craig, B. Barth, C. M. Beavers, S. J. Teat, G. Aromí, *J. Am. Chem. Soc.*, **2014**, *136*, 3869; f) R. Kulmaczewski, H. J. Shepherd, O. Cespedes, M. A. Halcrow, *Inorg. Chem.*, **2014**, *53*, 9809; g) R. Kulmaczewski, J. Olguín, J. A. Kitchen, H. L. C. Feltham, G. N. L. Jameson, J. L. Tallon, S. Brooker, *J. Am. Chem. Soc.*, **2014**, *136*, 878; h) S. Rodríguez-Jiménez, H. L. C. Feltham, S. Brooker, *Angew. Chem., Int. Ed.*, **2016**, *55*, 15067; i) C. Bartual-Murgui, C. Codina, O. Roubeau, G. Aromí, *Chem. – Eur. J.*, **2016**, *22*, 12767; j) I. Šalitroš, O. Fuhr, M. Ruben, *Materials*, **2016**, *9*, 585

[8] Most recent articles are a) I. A. Gural'skiy, S. I. Shylin, B. O. Golub, V. Ksenofontov, I. O .Fritsky, W. Tremel, *New J.Chem.,* **2016**, *40***,** 9012; b) J. E. Clements, J. R. Price, S. M. Neville, C. J. Kepert, *Angew. Chem., Int. Ed., **2016**, 55***,*** 15105; c) F. J. Valverde-Munoz, M. Seredyuk, M. Carmen Munoz, K. Znovjyak, I. Fritsky, J.-A. Real, *Inorg. Chem.,* **2016** *, 55,* 10654; d) Z. Setifi, A. Addala, J. Tao, N. Wannarit, C. Glidewell, F. Setifi, S. Youngme, *Inorg. Chem. Commun.,* **2016**, *68***,** 80; e) T. Kosone, T. Kitazawa, *Inorg. Chim. Acta,* **2016**, *439***,**159; f) J. Okabayashi, S. Ueno, T. Kawasaki, T. Kitazawa, *Inorg. Chim. Acta,* **2016**, *445***,** 17; g) Z. Yan, L.-F. Zhu, L.-W. Zhu, Y. Meng, Md N. Hoque, J.-L. Liu, Y.-C. Chen, Z.-P. Ni, M.-L. Tong, *Inorg. Chem. Front.,* **2017***, 4*, 921; h) L. Pineiro-Lopez, F. J. Valverde-Munoz, M. Seredyuk, M. Carmen Munoz, M. Haukka, J.-A. Real, *Inorg. Chem.,* **2017**, *56*, 7038; i) Y. Meng, Q.-Q. Sheng, Md N. Hoque, Y.-C. Chen, S.-G. Wu, J. Tucek, R. Zboril, T. Liu, Z.-P. Ni, M. Tong, *Chem. - Eur. J.,***2017**, *23***,** 10034; j) L. Pineiro-Lopez, F. Javier-Valverde-Munoz, M. Seredyuk, C. Bartual-Murgui, M. Carmen Munoz, J.-A. Real, *Eur. J. Inorg. Chem.,* **2018***,* 289

[9] P. King, J. Henkelis, C. Kilner, M. Halcrow, *Polyhedron*, **2013**, *52*, 1449.

[10] Y. Lin, S. Lang, *J. Heterocycl. Chem*, **1977**, *14*, 345.

[11] a) P. Guionneau, M. Marchivie, G. Bravic, J.-F. Létard, D. Chasseau, *Top. Curr. Chem.* **2004**, *234*, 97; b) M. Marchivie, P. Guionneau, J.-F. Létard, D. Chasseau, *Acta Cryst.* **2005**, *B61*, 25.

[12] a) E. Trzop, D. Zhang, L. Piñeiro-Lopez, F.J. Valverde-Muñoz, M. C. Muñoz, L. Palatinus, L. Guerin, H. Cailleau, J. A. Real, E. Collet, Angew. Chem. Int. Ed. Engl. 2016, 55, 8675; b) E. Collet, H. Watanabe, N. Bréfuel, L. Palatinus, L. Roudaut, L. Toupet, K. Tanaka, J.-P. Tuchagues, P. Fertey, S. Ravy, B. Toudic, H. Cailleau, Phys. Rev. Lett. 2012, 109, 257206 ; c) K.D. Murnaghan, C. Carbonera, L. Toupet, M. Griffin, M.M. Ditru, C. Desplanches, Y. Garcia, E. Collet, J.F. Létard, G. Morgan, Chem. Eur. J. 2014, 20, 5613.

[13] a) J.-F. Létard, P. Guionneau, L. Rabardel, J. A. K. Howard, A. E. Goeta, D. Chasseau, O. Kahn, *Inorg. Chem.* **1998**, *37*, 4432; b) J.-F. Létard, L. Capes, G. Chastanet, N. Moliner, S. Létard, J. A. Real, O. Kahn, *Chem. Phys. Lett.* **1999**, *313*, 115; c) J. F. Létard, *J. Mater. Chem.* **2006**, *16*, 2550; d) J. F. Létard, P. Guionneau, O. Nguyen, J. Sanchez Costa, S. Marcén, G. Chastanet, M. Marchivie, L. Goux-Capes, *Chem. Eur. J.* **2005**, *11*, 4582; e) N. Shimamoto, S.-S. Ohkoshi, O. Sato, K. Hashimoto, *Inorg. Chem.* **2002**, *41*, 678; f) J.-F. Létard, G. Chastanet, P. Guionneau, C. Desplanches, in Spin Crossover Materials: Properties and Applications, *Ed. Malcom A. Halcrow,* **2013**, John Wiley & sons, 475.

[14] R. Kulmaczewski, E. Trzop, L.J. Kershaw Cook, E. Collet, G. Chastanet, M.A. Halcrow, *Chem. Commun*. **2017**, *53*, 13268.

[15] G. Sheldrick, *Acta Crystallogr. Sect. C*, (71), **2015**, 3–8; G. M. Sheldrick, *Acta Crystallogr. Sect. A*, **2008**, *64*, 112.

[16] O. V Dolomanov, L. J. Bourhis, R. J. Gildea, J. A. K. Howard and H. Puschmann, *J. Appl. Crystallogr.*, **2009**, *42*, 339

[17] G.M. Sheldrick, 1996, *TWINABS.* University of Göttingen, Germany

[18] G. M. Sheldrick, *Acta Cryst*. **2015**, *A71*, 3

Received: ((will be filled in by the editorial staff))
Published online: ((will be filled in by the editorial staff))

## Entry for the Table of Contents

## Layout 1:

**((Key Topic))**

**Solvatomorphism-Induced 45 K Hysteresis Width in a Spin Crossover Mononuclear Compound**

This paper reports the drastic influence of solvatomorphism on magnetic thermal hysteresis of a spin-crossover complex $[Fe(3\text{-}bpp)_2][Au(CN)_2]_2$ : the hydrated compound presents a gradual spin-crossover whereas the solvent free one presents an hysteresis as large as 45 K accompanied by a structural transition and a reversible twinning. (Photo)magnetic characterizations are correlated with structural studies in temperature and under irradiation.

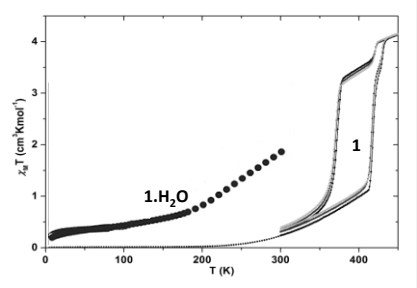


Abdelhak Djemel, Olaf Stefanczyk, Mathieu Marchivie, Elzbieta Trzop, Eric Collet, Cédric Desplanches, Rachid Delimi, Guillaume Chastanet

…….. Page No. – Page No.

**Keywords:** Coordination Chemistry / Spin-Crossover / Solvatomorphism / Hysteresis / aurophilic interactions / phase transition